Aperture Synthesis Thermography—A New Approach to Passive Microwave Temperature Measurements in the Body

NICOLA C. HASLAM, ANTHONY R. GILLESPIE, AND C. GLYN T. HASLAM

Abstract—**The radio astronomical technique of aperture synthesis is proposed for use in medical applications to give, noninvasively, a thermal image of a large fraction of the human body to a depth of several centimeters with no microwave irradiation. The principles of operation are illustrated by a practical design which could give a sensitivity of a few milli-Kelvin over a 50-cm field in a 10-s exposure.**

Applications of the proposed system include detection of cancers and other infections, and also real-time monitoring of the effects of hyperthermia on the surrounding tissue.

I. Introduction

THERE IS A growing need for a noninvasive method of measuring temperatures of small regions inside the human body, not only for the early detection of cancers and infected regions, but also for monitoring the effect of hyperthermia produced by microwave radiation. Infrared and high-frequency ($f > 10$ GHz) radiometers utilizing thermal blackbody radiation can only monitor effects near the surface due to the body's high optical depth at these wavelengths. Longer wavelength radiometers look deeper into the body, but suffer from low angular resolution and slow speed to monitor more than one area [1], [2]. Better resolution is possible using imaging techniques [3], but so far these have only been used on isolated organs and need a high-power source irradiating the object, although the authors do suggest that their methods could be used for thermography.

Aperture synthesis is widely exploited in radio astronomy [4], [5] to give much higher resolution than is possible with a single antenna, but has not yet been considered for thermography. We show in this paper that it is valid for this purpose. The modifications to standard synthesis are discussed, and in Section II, a practical system is shown which can detect deep-seated hot spots 1.5 K above ambient temperature, with a positional accuracy of a few millimeters. Section III gives a more detailed outline of the components of such a system, and some possible applications are given in Section IV.

Manuscript received October 12, 1983; revised March 14, 1984.

N. C. Haslam is at 24 Sandringham Dr., Wistaston, Crewe CW2 8JF, England.

A. R. Gillespie and C. G. T. Haslam are with the Max-Planck-Institut für Radioastronomie, Auf dem Hügel 69, D5300 Bonn 1, West Germany.

II. Aperture Synthesis Applied to Thermography

The fundamental principle of aperture synthesis as used in radio astronomy is that the distribution of amplitude and phase over an antenna's aperture is the Fourier transform of the source's brightness distribution. In order to synthesize a very large single dish, the aperture plane is sampled by pairs of small antennas connected together as phase-switched interferometers with one antenna used as a phase reference point. The antennas are usually along a line or in a 'Y' form, and the earth's rotation is used to sample the other coordinate. The antenna separation is then altered between successive days' observations to obtain full aperture-plane sampling. A Fourier transform is performed on the amplitude and phase at each sample point to give a picture of the sky brightness within the primary beam of the individual antennas.

The principles remain the same for thermography, but the basic parameters are different. A patient can only remain still (on a scale of a millimeter or two) for a short period, thus limiting the exposure time. Therefore, to achieve adequate sensitivity, all the necessary antennas must be present simultaneously. Clearly, earth rotation cannot be exploited, so either a fully sampled two-dimensional array must be built, similar to that in [3], or a line of antennas that can be rotated 180° around its center (180° rotation rather than 90° rotation may be essential if the patient is not in the far field of the individual antennas, as the Fourier components in the quadrants of the uv plane are no longer related by $T_a(-u,-v) = T_a^*(u,v)$, where u and v are the coordinates in the Fourier transform plane of the array—([5], eq. 7.6). The choice between the two- and one-dimensional arrays would be made on cost considerations, with the rotating array probably being cheaper. The picture size is set by computing considerations and the requirement that the whole of the area examined must be in the primary beam of all the individual antennas. The maximum resolution (Θ radians) is fixed by the largest antenna separation D, and the observing wavelength (λ) in the relation $\Theta = \lambda/D$. In practice, D cannot be much larger than the patient. The observing frequency must be below about 5 GHz to give penetration into the body, but the effective wavelength can be changed by using a high dielectric constant, low-loss material between the patient

0018-9480/84/0800-0829$01.00 ©1984 IEEE

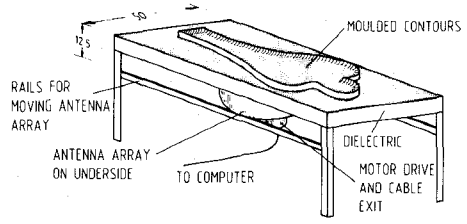

Fig. 1. A schematic view of a possible arrangement for an aperture synthesis thermograph.

TABLE
SYSTEM PARAMETERS

Frequency	915	1500	2450	3000	MHz
Resolution	1.49	0.91	0.55	0.45	cms
Number of antennae in array	12	19	30	37	
Bandwidth	100	200	400	500	MHz
R.m.s. noise in 10 second exposure	5.47	3.07	1.73	1.39	milli Kelvin
Time taken to see 1.5 K warmer layer below 2 mm skin, 1 cm fat and 4 cm muscle	6	9	57	222	seconds

Maximum antenna separation: 50 cm.
Distance from patient to antenna array: 12.5 cm.
Dielectric constant of table: 30.
System noise temperature: 300 °K + 300 °K from patient.

and antennas bringing a corresponding improvement in resolution. This also reduces reflection losses at the skin-to-air interface.

Fig. 1 shows a proposed system, with expected performance for different operating frequencies given in Table I. The patient lies on a dielectric table which is shaped, or has moveable shaped slabs on it for best contact with the patient's skin. A high dielectric constant cushion (or even a thin polythene envelope of warm water) could be used for both the patient's comfort and to give good contact between the patient and the table. The array consists of a line of dipoles mounted on the underside of another piece of rotatable dielectric, which can be moved under the appropriate part of the table (with good contact) for the desired examination. The amplitude and phase of the thermal emission from the patient are fed to a minicomputer which performs a Fourier transform, and the image of the part of the patient over the array is displayed on a visual display unit at the end of each exposure. The image can be stored on a floppy disc for future reference or for comparison with images made during successive examinations.

III. System Parameters and Components

A. Spatial Resolution

Resolution is used here in the sense of the full-beamwidth given by $\Theta = \lambda/D$. For an array at a distance l from the object being examined, the resolution is then $r = \lambda l/D$ cm, expressed in terms of distance in the patient (see Fig. 2). D/l can only have a value between 0.5 and 5 for practical reasons, with 4 being a reasonable value, but the wavelength can be be reduced by a factor of 5.5, using a dielectric with $\epsilon_r = 30$ (e.g., HiK from Emerson & Cuming, Canton, MA 02021) between the patient and the array

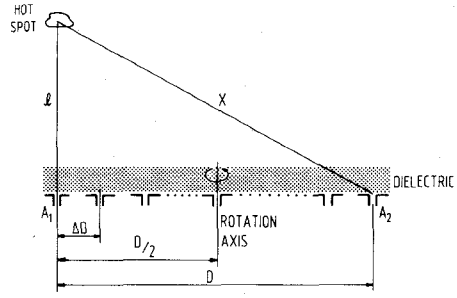

Fig. 2. A schematic side view of the array showing geometrical dimensions.

giving a corresponding improvement in resolution. This gives a resolution of

$$r = \frac{cl}{fD\sqrt{\epsilon_r}} \tag{1}$$

and is given in Table I for several frequencies with $D/l = 4$. The use of a dielectric has two further advantages: 1) the small antennas can be mounted on a rotating piece of it, enabling stripline techniques to be used in their construction, and perhaps also in the local oscillator supply, and signal amplifier and mixer chains and 2) suitable shaping of the material to give good contact to the patient's body shape will considerably improve the matching of the body to the antennas as there is then no longer a skin-to-air interface (high-to-low ϵ_r).

The resolution given above, which is of the order of 0.5 to 2.5 cm for 3 GHz $> f >$ 1 GHz, is *not* the error in the determination of the position of the hotter region as beam-fitting techniques can give the position of small sources to within 0.1 beamwidths even when the signal-to-noise ratio of the signal is only 5 : 1.

B. Operating Frequency

The choice of frequency must consider four factors affecting the visibility of a hot region of fixed size inside the body.

1) The radiation's penetration ($1/e$) depth in tissue increases with wavelength, the absorption coefficient is given approximately by

$$\alpha = 2.2 \times 10^{-5}\sqrt{f} + 0.1 \tag{2}$$

over the frequency range 100 MHz to 3 GHz (this is derived empirically from the data in [6]).
2) The hot spot's optical depth increases with frequency, giving an increase in effective temperature rise above the surroundings.
3) Beam dilution effects reduce the hot spot's effective temperature by the ratio of its cross-sectional area to that of the synthesized beam.
4) The reflections at interfaces inside the body between materials of different permittivities cause losses.

Quantifying effects 1), 2), and 3), and using (1) and (2), leads to a relation for the change in temperature seen at the

skin's surface

$$\Delta T_e = \Delta T \epsilon_r \left(\frac{Dkf}{lc}\right)^2 \left[1 - \exp - \left(2.2 \times 10^{-5} \sqrt{f} + 0.1\right) k\right] \cdot \exp - \left(2.2 \times 10^{-5} \sqrt{f} + 0.1\right) b \quad (3)$$

where

ΔT = hot spot's actual temperature rise above its surroundings,
k = the diameter of the hot spot, assumed to be a uniform disc, also of thickness k,
b = the depth of the hot spot below the body surface.

The value of ΔT_e for several parameters is shown in Fig. 3(a). Fat has been ignored here because its absorption coefficient is much lower than α above, but shows the same variation with frequency. The effect of mismatches at boundaries due to effect 4) above can be seen in Fig. 3(b), which gives the temperature measured just outside the skin for a 1.5-cm-thick layer of hotter material seen through 2 mm of skin and layers of muscle and fat. This is based on the relation (see [7])

$$\Delta T_e = \Delta T \left[1 - \exp\left(-\frac{z_t}{d_t}\right)\right] \exp\left(-\frac{z_f}{d_f}\right) \cdot e_{fs} \cdot \exp\left(-\frac{z_s}{d_s}\right) \cdot e_{so} \cdot \exp\left(-\frac{z_m}{d_m}\right) \cdot e_{mf} \quad (4)$$

where

z_t, z_f, z_s, z_m are the thicknesses of the layers of tumor, fat, skin, and muscle, respectively,
d_t, d_f, d_s, d_m are the $1/e$ penetration depths of the materials at a given frequency,
e_{fs}, e_{so}, e_{mf} are the emissivities from fat to skin, skin to outside the body, and muscle to fat.

Consideration of Fig. 3 shows that, for small hot spots, higher frequencies are better, until either ΔT_e levels off or (2) breaks down (> 3 GHz), while for larger hot areas, the lower frequencies are better. Therefore, the choice of operating frequency, within the range 900 to 3000 MHz, must depend on the particular application being considered.

Closely related to the operating frequency is the usable bandwidth. This must be sufficiently small for the phase difference between signals at the antennas with the largest separation, A_1 and A_2 in Fig. 2, not to change by more than 90° across the band for points at the edge of the picture area. Taking the picture area to be the same as the antenna array area and directly over it, we come to the relation

$$\Delta f < \frac{f^2}{4c} \frac{xl}{(x-l)} \quad (5)$$

where Δf is the bandwidth and $x = \sqrt{l^2 + D^2}$. This is a very weak constraint, varying from 11 to 40 percent of the operating frequency over the range 915 to 3000 MHz, and the bandwidths given in Table I are less than this.

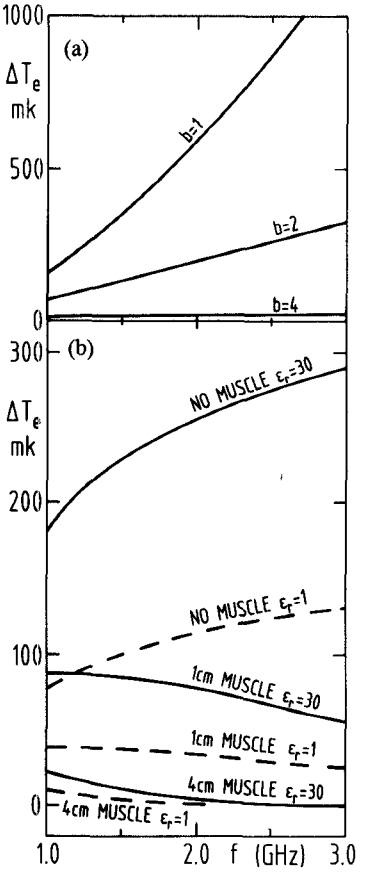

Fig. 3. The temperature difference seen just into a dielectric for (a) an isolated hot spot of diameter 1 cm with $T = 1.5°$K seen through various thicknesses of muscle; (b) a layer of warmer material seen under 2 mm of skin and 1 cm of fat for various thicknesses of muscle for air ($\epsilon_r = 1$) and dielectric ($\epsilon_r = 30$). In both cases, the hotter material has the electrical properties of muscle.

C. The Antenna Array

It was shown in Section II that all necessary antenna spacings must be present simultaneously. The number of antennas is determined by the minimum separation between antennas (ΔD) for the lowest Fourier component to have a radius larger than the picture size (e.g., [5], pp. 129 and 177). In our case, the restriction is that $\lambda/\Delta D > \phi$, where ϕ is the angle subtended by the examined area at one element of the array, with $\phi = \tan^{-1}(D/l)$. Expressed in terms of frequency we have

$$\Delta D < \frac{c}{f}\left[\sqrt{\epsilon_r} \tan^{-1}\left(\frac{D}{l}\right)\right]^{-1} \quad (6)$$

and the number of antennas

$$n = \frac{D}{\Delta D} + 1. \quad (7)$$

For $D/l = 4$, ΔD is of the order of one or two centimeters, so dipoles with suitable balancing networks are ideal as the individual antennas. The patient is in the near field of the array so it is not possible to reduce the number of antennas by the usual procedure of having unequally spaced antennas separated by multiples of ΔD and reconstructing the whole aperture using combinations of these. Although this

increases the array costs, it is offset to some extent by the fact that the path compensators and phase rotators used in astronomy are unnecessary and the data rate is not too high for a small computer to handle. It should also be noted that care must be taken with the Fourier transform as the signals going to each antenna pair will not have equal electrical path lengths or equal attenuation, but regular calibration using measurements of artificial dielectric and water sources of known, nonambient temperature should remove this problem.

D. Preamplifiers

Many preamplifiers are necessary, as all antenna pairs are present, so they must be relatively inexpensive. Since the array looks at a 300-K patient, this is the lowest possible overall system noise temperature with a perfect amplifier. With the calibration methods discussed in the Appendix, a directional coupler, circulator, and filter are needed between the dipoles and preamplifiers giving a small degradation in system noise temperature. A simplified sketch of the system is shown in Fig. 4. For our calculations, we have assumed a system noise temperature of 600 K = 300-K patient + 300-K amplifier, since such amplifiers are readily available at low cost.

E. The Correlators and Continuous Calibration

The amplitude (A) and phase (ϕ) are measured as sine (S) and cosine (C) terms, where $A^2 = S^2 + C^2$ and $\phi = \tan^{-1}(S/C)$, by cross correlation of the signal from the central receiver with that of a receiver at the appropriate spacing for each of the spacings. In the system proposed, the bandwidths are much larger than those used in astronomical synthesis; the correlators, then, must be carefully designed so that the relative phase between inputs is less than a few degrees across the whole bandwidth (200 MHz for the 1.5-GHz system). In addition, they need at least a 40-dB dynamic range (1 mK to 10 K). This specification can be achieved by the use of linear multipliers and by 180° broad-band phase switching in one of the IF inputs (see Fig. 5). When synchronous demodulation is applied, this removes the 5-percent or so square-law response inherent in the multipliers at higher signal levels and simultaneously corrects for zero drift in the multipliers and following voltage-to-frequency convertors. These convertors, in conjunction with buffered counters, act as integrators. Gain calibration for each channel is derived by a modulated noise source switched at half the phase inversion rate and which is weakly (−25 dB) but *coherently* coupled into the input circuit of each preamplifier (see Fig. 4). Software demodulation (see the Appendix) makes possible real-time correction, during the analysis, for system drifts of phase and amplitude and provides engineering monitoring of possible system malfunctions.

Broad-band 45-dB dynamic correlation systems, with long-term errors <1-percent gain and <1° of phase after calibration, have been in regular service on the MPIfR 100-m telescope since 1974 in the 0.4–10.7-GHz range (see, for example, [8] and [9]).

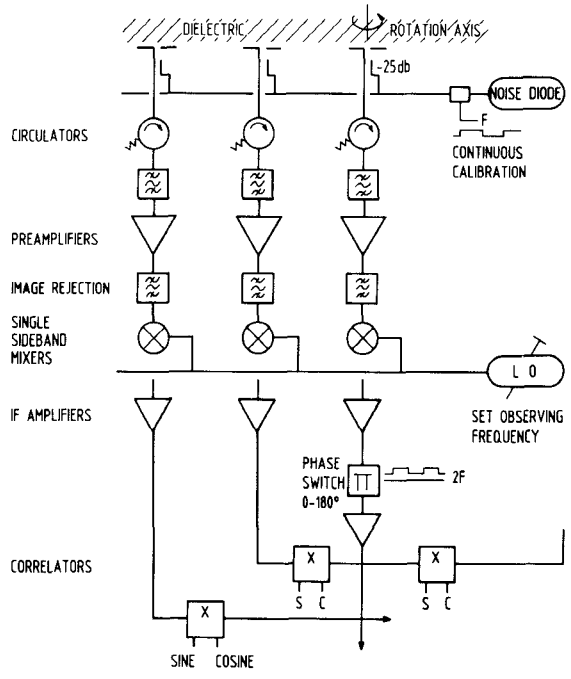

Fig. 4. A simplified sketch of the receiving system showing connections for three correlators and other essential components. The broad-band phase switch in the central receiver is reversed at 20-ms intervals and the output of the noise source is modulated by a pin switch at half this rate. It is important *not* to continuously interrupt the dc supply of the avalanche noise diode, otherwise the noise output stability will be seriously impaired.

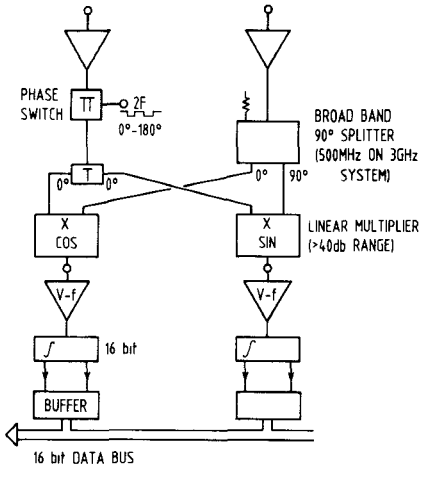

Fig. 5. The basic broad-band correlator element. In practice, a single broad-band phase switch can be incorporated into the IF chain of the central receiver, greatly simplifying the system electronics as is sketched in Fig. 4.

F. Fourier Transform and Image Matrix

During the rotation of the array, we need to collect $D\pi/\Delta D$ samples each of $N-1$ amplitudes and phases to match the minimum separation limit calculated in Section III-C. For the 1.5-GHz system, this gives 57 samples each of 18 amplitudes and phases. We have chosen 64 samples each lasting 160 ms in the software demodulation example shown in the Appendix. As the array rotates, the amplitude and phase information is interpolated into a u, v matrix, and the continuous calibration corrections described in the Appendix are computed and applied at the end of the scan

directly into the u, v array. This array is then Fourier transformed to form the image. This transform may well require special-purpose hardware to take full advantage of the short 10-s exposure time required by the receivers.

The image matrix requires a minimum of two points per resolution element [10] which, for the 1.5-GHz system, is 0.91 cm (Table I) giving a grid point separation of 0.45 cm. A 50-cm square image then needs a matrix of 111×111 points. If each element has 2-byte accuracy (1 in 65536), we can provide a temperature range of 10°K relative to some conveniently chosen zero for the image, with an accuracy of 0.15 mK due to round-off. Such an image would require 25K bytes, including identification and calibration information and sixteen such images could be stored on a single 0.5-Megabyte floppy disk, including patient case history details. This would give a convenient and cheap filing method for hospital use, allowing later off-line inspection by a consultant and eventual transfer to mass storage for large sample statistical analysis.

The image matrix could well have the format described in [11], which is very efficient in computer time when used with two-dimensional regridding and interpolation routines. These operations will be essential for comparing pictures taken on different days since the patient will not lie in exactly the same place, so superposition, shifts of scale, translation, and rotation will be required before detailed comparison can be made. Suitable software and necessary algorithms, including techniques for combining overlapping images, have been described, in an astronomical context, in [12].

Care will be needed in the choice of a suitable computer to drive the system, but the data rates are not excessive and should be well within the scope of a special-purpose multimicro system.

IV. Applications and Uses

A. Cancer Detection

The area surrounding carcenogenic activity usually shows an excess of temperature; this effect is extended to a larger volume by the flow of blood from the excess of blood vessels found around the cancer sites. This has the effect of filling the beam of the thermograph and producing more detectable signals than that expected for the cancerous area alone. One should be able to detect cancerous activity with a local excess of only 1.5°K at depths greater than 4 cm in muscle and much greater depths in fatty tissue (see Table I).

Routine screening of people for cancer or other infections could be implemented without any danger of side effects since the method is *passive* and noninvasive. The images and patient details could easily be stored on a floppy-disc filing system and copied to mass storage for large-scale statistical analysis at a later date.

B. Hyperthermia Monitor

One of the most useful applications of the machine could be to provide a real-time image of the temperature distribution around a site being given hyperthermia treatment. For this purpose, it would be necessary to time-share the image scanning process with the application of hyperthermia power, while providing adequate protection for the receiver preamplifier stages. If the time-sharing intervals were small, say 0.1 s, the cooling effects of the bioheat transport mechanisms around the area would be negligible; thus, the thermogram would represent the true temperature distribution during the hyperthermia process. This would greatly aid the preferential destruction of the cancers and the implementation of high-resolution phased-array hyperthermia systems. This has been suggested in [13], although these authors imply that only low-resolution thermography is possible, whereas our system should give a high enough resolution to match the size of the area warmed by the hyperthermia treatment.

C. Detection of Infected Organs and Areas

The machine should provide a simple, practical, and noninvasive way of detecting internal areas where a local temperature excess may indicate a site of abnormal biological activity due to infection. If the image of the area is processed by a suitable Fourier filter, it is possible to remove extended background components and so enhance the image contrast at these sites.

D. Depth Estimation

Since the measured temperature for a hot spot varies quite differently with depth for small changes of observing frequency, in the range 1–3 GHz, it should be possible to estimate the depth of the activity by comparing images taken at different frequencies, after normalizations for the effects of resolution changes, as a function of frequency.

E. Observations in Transmission

A further technique which might be useful is to shine a narrow-band noise source through the body. The power required for an adequate signal is quite small (1 mW) and does not represent a health hazard. This signal would be blinked and detected synchronously in the computer software. The method may reveal variations in the opacity of the tissue as a function of frequency which can be detected by image comparison and may be found in clinical practice to correlate with abnormalities.

V. Conclusions

The use of aperture synthesis techniques enables thermal pictures to be made of large parts of the body in a short time by passive, noninvasive methods. The optimum frequency range is 0.9–3 GHz. The system sensitivity should be such that small, locally warm regions can be detected to a depth of several centimeters into the body.

The proposed system can be constructed from existing proven elements, but careful design of the antenna array will be needed to minimize coherent cross talk between the separate channels.

Acknowledgment

The authors wish to thank Dr. J. Baker of the Manchester University Physics Department for first calling our

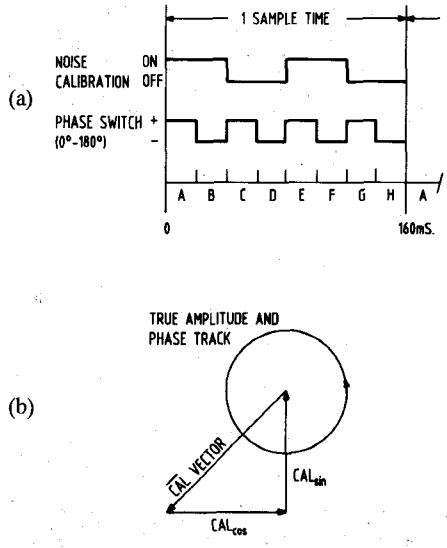

Fig. 6. (a) The system switching sequence used by the software demodulation process described in the Appendix. The mean reference information is used in the analysis to correct for instrumental drifts in gain and phase and can be used to monitor channels for calibration and maintenance purposes. (b) The mean reference signal $\overline{\text{Cal}}$, averaged over the exposure time, must be subtracted in order to form the correct sine and cosine amplitude vectors.

attention to the Microwave Thermography problem, and G. Ediss of the MPIfR for helpful discussions.

Appendix

Software Synchronous Detection

The method of deriving sine and cosine terms in the correlators is shown in Fig. 5, which expands the lower part of Fig. 4 for two antennas. The system is calibrated by injecting a noise signal in at a known low level (~ 40 K) directly after each antenna so that the observations are made continuously but with slight degradation in noise figure during those parts of the cycle with the extra noise signal. The switching cycles of the noise source and phase switch are shown in Fig. 6(a) for one integration time split into equal time intervals A to H.

Denoting the mean power received during a given time interval in the cycle by the appropriate letter, the sine and cosine signals can both be demodulated by evaluating the following expressions, for each of the sine and cosine channels of each correlator:

$$(A-B)+(C-D)+(E-F)+(G-H)=\text{Sig}$$
(sine or cosine term)

$$(A-B)-(C-D)+(E-F)-(G-H)=\text{Cal}$$
(sine or cosine term).

Two broad-band multipliers in quadrature give sine and cosine correlations as is shown in Fig. 5.

Then we compute the following:

$$\text{Reference Cal}=\sqrt{(\text{Cal}_{\cos})^2+(\text{Cal}_{\sin})^2}$$

$$\text{Reference phase}=\tan^{-1}[\text{Cal}_{\sin}/\text{Cal}_{\cos}]$$

$$\text{Mean Cal}\left(\overline{\text{Cal}}\right)=\sum \text{Reference Cal}/\text{Number of samples}$$

$$\text{Corrected amplitude}=\left[\sqrt{(\text{Sig}_{\cos})^2+(\text{Sig}_{\sin})^2}-\overline{\text{Cal}}\right]\times\left[\text{Standard Cal}/\overline{\text{Cal}}\right]$$

$$\text{Corrected phase}=\tan^{-1}[\text{Cal}_{\sin}/\text{Cal}_{\cos}]-[\text{Ø Chan}+\text{Reference phase}].$$

ϕ Chan is a calibration factor determined for each correlator and allows for electrical path differences through each receiver channel. $\overline{\text{Cal}}$ must be subtracted to correct for the vector offset in the amplitude and phase determination due to the calibration noise signal (see Fig. 6b).

References

[1] A. H. Barrett, P. C. Myers, and N. L. Sadowsky, "Detection of breast cancer by microwave radiometry," *Radio Sci.*, vol. 12 (supplement), pp. 167–171, 1977.
[2] S. Osterrieder and G. Schaller, "A microwave radiometer for medical applications," *Frequency*, vol. 37, pp. 7–12, 1983 (in German).
[3] G. Peronnet, Ch. Pichot, J. Ch. Balomey, L. Jofre, A. Izadnegahdar, C. Szeles, Y. Michel, J. L. Guerquin-Kern, and M. Gautherie, "A microwave diffraction tomography system for biomedical application," in *Proc. 13th Eur. Microwave Conf.*, 1983, pp. 529–533.
[4] M. Ryle and A. Hewish, "The synthesis of large radio telescopes," *Monthly Notices of the Royal Astronomical Society*, vol. 120, pp. 220–230, 1960.
[5] W. N. Christiansen and J. A. Högbom, *Radio Telescopes*. Cambridge University Press, 1969.
[6] C. C. Johnson and A. W. Guy, "Nonionizing electromagnetic wave effects in biological materials and systems," *Proc. IEEE*, vol. 60, pp. 692–718, 1972.
[7] J., Edrich, "Centimeter and millimeter wave thermography—A survey on tumous detection," *J. Microwave Power*, vol. 14, pp. 95104, 1979.
[8] C. G. T. Haslam, U. Klein, C. J. Salter, H. Stoffel, W. E. Wilson, M. N. Cleary, D. J. Cooke, and P. Thomasson, "A 408 MHz all-sky survey. I. Observations at southern declinations and for the north polar region," *Astron. Astrophysics*, vol. 100, pp. 209–219, 1981.
[9] D. T. Emerson, U. Klein, and C. G. T. Haslam, "A multiple beam technique for overcoming atmospheric limitations to single-dish observations of extended radio sources," *Astron. Astrophysics*, vol. 76, pp. 92–105, 1979.
[10] R. N. Bracewell and J. A. Roberts, "Aerial smoothing in radio astronomy," *Australian J. Phys.*, vol. 7, pp. 615–640, 1954.
[11] C. G. T. Haslam, "NOD 2: A general system of analysis for radioastronomy," *Astron. Astrophysics Suppl.*, vol. 15, pp. 333–335, 1974.
[12] C. G. T. Haslam, N. C. Haslam, and D. T. Emerson, "NOD 2: A generalised system of data analysis for astronomy which has application to image processing," *Technischer Bericht 56 des Max-Planck-Instituts für Radioastronomie Bonn*, 1980 (in English).
[13] M. Melek, A. P. Anderson, J. Conway, and B. H. Brown, "Three-dimensional phantom measurements validating the use of phased arrays for deep-seated tumor irradiation," in *Proc. 13th Eur. Microwave Conf.*, 1983, pp. 865–876.

Nicola C. Haslam was born in Nantwich, England, in 1962. She was awarded an Honors B.Sc. in physics by Manchester University, England, in 1983. She has an active interest in the application of physics to biology and medicine.

Anthony R. Gillespie was born in Kent, England, on October 18, 1947. He received the B.Eng. degree from Liverpool University in 1970, and

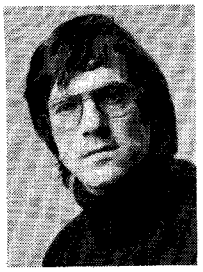

has spent two years working for Marconi Radar Systems Ltd. as a radar engineer. He was awarded the Ph.D. degree by Cambridge University in 1974 for work on faint radio sources using aperture synthesis telescopes at the Mullard Radio Astronomy Observatory.

Since then, he has worked in the field of millimeter and submillimeter astronomy, observing with hetrodyne systems he has developed at frequencies of up to 460 GHz, both at Queen Mary College, England, until 1977, and at the MPIfR Bonn, West Germany.

C. Glyn T. Haslam was born in Bolton, England, in 1936. He was awarded an Honors B.Sc. degree in physics by Manchester University, England, in 1958.

He joined the staff of the Nuffield Radio Astronomy Laboratories, Jodrell Bank, where he obtained the Ph.D. degree in physics in 1962, working on the application of digital methods in radio astronomy. He continued this work until 1970, when he joined the staff of the Max Planck Institut für Radioastronomie in Bonn, where he worked on the design and development of the receiving, data collection, and analysis methods which were being installed on the new 100-m telescope at Effelsberg. From 1962, he organized and was involved with several large-scale decimetric galactic background surveys which are being used to study the large-scale energy distribution in our galaxy. He is currently Group Leader of the Continuum Astronomy Group at the MPIfR, and continues to develop new measuring and analysis techniques.

Microwave-Induced Thermoacoustic Effect in Dielectrics and Its Coupling to External Medium—A Thermodynamical Formulation

THEODORE C. GUO, SENIOR MEMBER, IEEE, WENDY W. GUO, SENIOR MEMBER, IEEE, AND LAWRENCE E. LARSEN, SENIOR MEMBER, IEEE

Abstract—**A thorough formulation of electromagnetic wave interaction with biological systems is presented. The thermodynamic process of the microwave-induced thermoacoustic generation is clearly defined. Couplings of the acoustic and thermal energies to the surrounding medium are included through consideration of discontinuities of thermodynamical variables and microwave exposure. Contrary to prior analyses, it is shown that acoustic waves may be generated by pulsed microwaves, even in the absence of inhomogeneity of microwave absorption, owing to discontinuities of thermodynamical variables and microwave exposure conditions across the interface. General equations for the thermoacoustic waves are derived, and the validity of the first-order linear approximation is estimated in terms of its percentage error. For a system with water as the absorbing dielectric interfacing with air of 1 atmosphere pressure, the first-order approximation becomes invalid for a peak specific absorption rate greater than 13 kW/gm.**

Manuscript received October 12, 1983; revised March 8, 1984. This work was supported in part by the Walter Reed Army Institute of Research through the U.S. Army Medical R&D Command under the U.S. Naval Sea Systems Command Contract N00024-83-C-5301.

T. C. Guo and W. W. Guo are with the Johns Hopkins Applied Physics Laboratory, Laurel, MD 20707.

L. E. Larsen is with the Department of Microwave Research, Walter Reed Army Institute of Research, Washington, DC 20012.

I. Introduction

THERMOACOUSTIC WAVES generated by pulsed microwaves have been cited as a mechanism for microwave hearing [1]–[6]. This effect has been experimentally shown to require an intact cochlea and 8th cranial nerve with a perceptional threshold near that of bone conduction. These facts imply that acoustic waves are transduced in the animal's skull by pulsed microwaves, then transmitted to the Organ of Corti by bone conduction. More recently, it has been demonstrated that acoustic waves are transduced in dielectric objects simulating the ocular lens when exposed to pulsed microwaves [7]. The putative effect has also been cited as the operant mechanism for cellular damage in studies of the murine ocular lens *in vitro* [8]. Several theories on the microwave auditory mechanism have been reviewed and compared by Lin [6]. Among them, it was found that only the thermoelastic mechanism could produce elastic waves of magnitude large enough to explain the experimental observations.

0018-9480/84/0800-0835$01.00 ©1984 IEEE